JACS
JOURNAL OF THE AMERICAN CHEMICAL SOCIETY
Article
pubs.acs.org/JACS

Strong Metal–Support Interactions between Gold Nanoparticles and ZnO Nanorods in CO Oxidation

Xiaoyan Liu,[†] Ming-Han Liu,[†] Yi-Chia Luo,[†] Chung-Yuan Mou,*[,†] Shawn D. Lin,[‡] Hongkui Cheng,[‡] Jin-Ming Chen,[§] Jyh-Fu Lee,[§] and Tien-Sung Lin[∥]

[†]Department of Chemistry, National Taiwan University, Taipei 10617, Taiwan
[‡]Department of Chemical Engineering, National Taiwan University of Science and Technology, Taipei 106, Taiwan
[§]National Synchrotron Radiation Research Center, Hsinchu 30076, Taiwan
[∥]Department of Chemistry, Washington University in St. Louis, St. Louis, Missouri 63130, United States

Supporting Information

ABSTRACT: The catalytic performances of supported gold nanoparticles depend critically on the nature of support. Here, we report the first evidence of strong metal–support interactions (SMSI) between gold nanoparticles and ZnO nanorods based on results of structural and spectroscopic characterization. The catalyst shows encapsulation of gold nanoparticles by ZnO and the electron transfer between gold and the support. Detailed characterizations of the interaction between Au nanoparticles and ZnO were done with transmission electron microscopy (TEM), X-ray photoelectron spectroscopy (XPS), X-ray absorption spectroscopy (XAS), electron paramagnetic resonance (EPR), and FTIR study of adsorbed CO. The significance of the SMSI effect is further investigated by probing the efficiency of CO oxidation over the Au/ZnO-nanorod. In contrast to the classical reductive SMSI in the TiO_2 supported group VIII metals which appears after high temperature reduction in H_2 with electron transfer from the support to metals, the oxidative SMSI in Au/ZnO-nanorod system gives oxygen-induced burial and electron transfer from gold to support. In CO oxidation, we found that the oxidative SMSI state is associated with positively charged gold nanoparticles with strong effect on its catalytic activity before and after encapsulation. The oxidative SMSI can be reversed by hydrogen treatment to induce AuZn alloy formation, de-encapsulation, and electron transfer from support to Au. Our discovery of the SMSI effects in Au/ZnO nanorods gives new understandings of the interaction between gold and support and provides new way to control the interaction between gold and the support as well as catalytic activity.

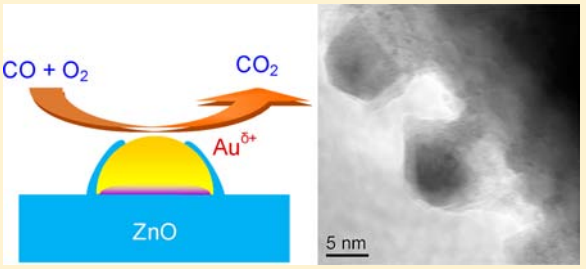

INTRODUCTION

CO oxidation on a supported gold nanocatalyst has been a paradigmatic problem in catalysis in the last two decades.[1,2] The apparently simple reaction is difficult to understand however because many factors, like the size of the gold particle size, the valence state of gold, and the interaction with the support, would influence dramatically the activity of the catalysts. These factors are difficult to isolate because they are normally intertwined together.[3−5] In particular, the nature of metal–support interaction is often difficult to elucidate. For example, high temperature pretreatment of catalysts would often change both the size (sintering) and the nature of metal–support interaction.[3,4,6] One would then like to have model systems where the sizes of the gold nanoparticle can remain unchanging during the pretreatment and reaction.[7] One way to do this is to develop yolk-shell type gold nanoparticles as model catalyst for support-effect studies.[8−11] The confined Au nanoparticles are uniform in size and sintering-resistant, which is particularly useful for weakly interacting supports such as carbon and silica. The approach, however, depends on our ability to make the required hollow metal oxides with precisely size-controlled gold inside which is often difficult.

We decide to approach the problem of studying support effect of gold by searching for the other limiting case—the strong metal–support interaction (SMSI). If SMSI is realized, the gold nanoparticles would remain constant in size (sintering resistant) once prepared because of the very strong interaction with support. Careful studies on the electronic interaction between support and metal can then be studied *in situ*. The classical SMSI effect as discovered by Tauster et al.,[12] on TiO_2 supported group VIII metal, was characterized by a dramatic encapsulation of metal by support and electron transfer from support to metal after reduction in H_2 at a higher temperature. Since then, a large number studies in catalysis and surface science have been reported, and it has been extensively demonstrated that the SMSI in supported group VIII metal play a significant role in affecting catalytic performances.[13−18] But supported gold is normally not regarded as a candidate for

Received: April 6, 2012
Published: May 21, 2012

   dx.doi.org/10.1021/ja3033235 | J. Am. Chem. Soc. 2012, 134, 10251−10258

SMSI because Au has a lower work function and surface energy and decoration of Au by the support oxide had not been observed. It has been suggested that the SMSI effect cannot exist in the supported gold systems.[19,20]

Here, we report the first evidence of SMSI between gold nanoparticles and ZnO nanorods based on the results of structural characterizations and spectroscopic studies. Under oxidative treatment, the catalyst shows both encapsulation of gold nanoparticles by ZnO and the electron transfer from Au to ZnO. The significance of the SMSI effect is further investigated in probing the efficiency of CO oxidation by tuning the metal–support interaction with oxidation–reduction cycle. These structural and activity studies allow us to obtain new insights into the nature of interaction between gold and the support, and furthermore, the results will provide a new way to study the catalytic mechanism of supported gold catalysts.

RESULTS

Sample Preparation. The ZnO-nanorod was synthesized by a room temperature solution synthesis method reported by Zeng and co-workers.[21] Its morphology is shown in Figure S1. The ZnO nanorods were several micrometers in length and 89 nm in average diameter (Figure S1a-c). The X-ray diffraction (XRD) pattern (Figure S1d) indicates that the nanorods exhibited a typical wurtzite structure.[22] The selected area electron diffraction pattern (Figure S1e) from an arbitrarily selected single ZnO nanorod illustrated a single rod was made of single crystal. Gold nanoparticles were deposited onto the surface of ZnO by deposition-precipitation (DP) method by tuning the pH value of the solution. The loading of Au was at 4.9 wt %, which is denoted as Au/ZnO-nanorod. When studying the interaction between gold and ZnO nanorods by XANES and EXAFS, in order to have good signal-to-noise (*S*/*N*) ratio, the loading of Au was increased to 20.8 wt %, which is denoted as 20Au/ZnO-nanorod.

Transmission Electron Microscopy. High-resolution transmission electron microscopy (HRTEM) (Figure 1a-b and Figure S2a) showed that the gold particles were small after pretreatment at 200 °C under flowing oxygen. The average particle size of gold was 3.9 nm (Figure S3a) which is just in the optimum size range (3–5 nm) of gold nanoparticles for high catalytic activity of CO oxidation.[7,23,24] The hemispherical shape of the particles, as typically found in Au/TiO_2,[25] indicates a pretty strong interaction between gold and ZnO. Surprisingly, we observed zinc oxide migrated onto the top surfaces of gold nanoparticles (Figure 1c-d and Figure S2b) after the Au/ZnO-nanorod was pretreated at 300 °C under flowing oxygen atmosphere. As shown in Figure 1d, the lattice spacing of the thin layer of ZnO encapsulating the gold nanoparticles is 0.26 nm which is consistent with the (002) plane of ZnO. The average particle size of gold nanoparticles remained at 3.4 nm (Figure S3b) which is similar to that of the sample pretreated at 200 °C where encapsulation has not occurred yet. This phenomenon is similar to the classical SMSI reported in titania-supported group VIII system when pretreated at 500 °C and above under hydrogen atmosphere.[12,13,26] However, the encapsulation phenomenon has not been reported in any transition metal oxide supported gold systems. Then, we further pretreated the catalyst under H_2 atmosphere and found that the thin layer of ZnO retreated from the surface of gold nanoparticles (Figure 1e-f and Figure S4) without much sintering (average size at 4.3 nm, as shown in Figure S3c). The reversible mass transport phenomenon is also in good agreement with the classical SMSI.[12,13] Although about 10% mismatch exists between the lattice spacing of Au (111) and ZnO (002),[27,28] as shown in Figure S4, there are still some epitaxial interactions between gold and ZnO, and some gold nanoparticles even sunk under the surface of the ZnO support with hydrogen treatment.

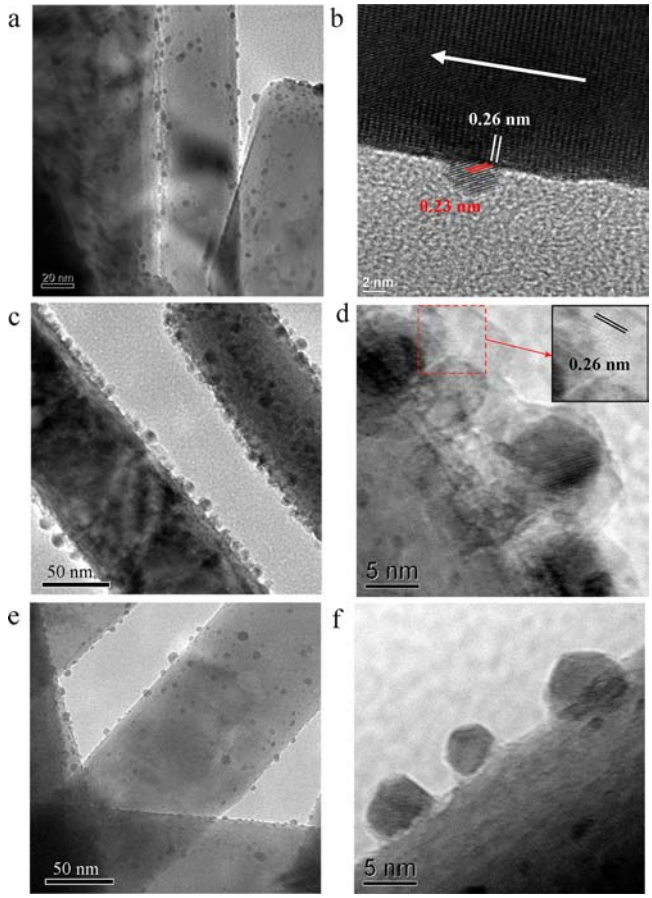

Figure 1. HRTEM images of the Au/ZnO-nanorod catalysts pretreated at 200 °C (a-b) and 300 °C (c-d) in 10% O_2/He (flow rate: 30 mL•min^{-1}) for 1 h and 300 °C in H_2 (flow rate: 30 mL•min^{-1}) for 1 h (e-f).

In Situ DRIFTS Studies of CO Adsorption. Besides the migration of support over the top of gold, the electronic interaction between Au and ZnO is also investigated. We chose *in situ* diffuse reflectance infrared Fourier transform spectroscopy (DRIFTS) to measure the adsorbed CO to probe the surface chemical property of the gold on ZnO nanorods. As shown in Figure 2a, a strong absorption band of CO positioned at 2101 cm^{-1} appeared on the Au/ZnO-nanorod sample dried at 60 °C which was ascribed to CO adsorbed on metallic gold.[29] With increasing pretreatment temperature, the CO absorption band blue-shifted and accompanied by a decrease in intensity. The decreased intensity of the bands may be ascribed to the lower CO coverage caused by the gradual encapsulation of gold nanoparticles by ZnO under increasing pretreatment temperature. For the surface of Au/ZnO pretreated at 300 °C under oxygen atmosphere, the CO adsorption band is shifted to 2113 cm^{-1}, which indicated that the surfaces of gold nanoparticles are slightly positively charged.[30] That is, electron transfer from gold nanoparticles to the support has occurred.[31,32] The band due to cationic gold (Au(I) or Au(III)) positioned at 2145–2200 cm^{-1} was not observed.

dx.doi.org/10.1021/ja3033235 | J. Am. Chem. Soc. 2012, 134, 10251–10258

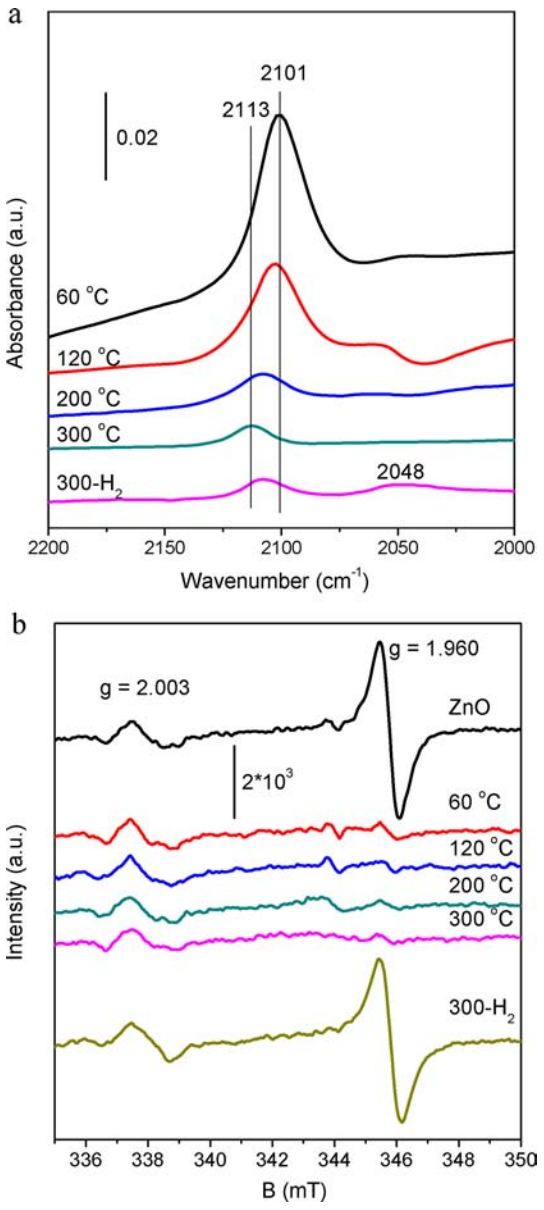

Figure 2. (a) *In situ* DRIFT spectra of adsorbed CO and (b) EPR spectra of Au/ZnO-nanorod catalysts pretreated under O_2 atmosphere at 60 °C, 120 °C, 200 °C, and 300 °C and followed by pretreatment under H_2 atmosphere at 300 °C.

After further pretreatment under hydrogen reduction, the CO adsorption band retreated to 2108 cm^{-1} which was the same as that of Au/ZnO pretreated at 200 °C under O_2 flow. At the same time, one more absorption band appeared at 2048 cm^{-1} which can be assigned to CO adsorbed on a negatively charged gold surface.[29] This manifested that the surface atoms of the gold nanoparticles regained some electrons after high temperature reduction. Thus, our *in situ* DRIFTS studies demonstrate that an electron transfer takes place reversibly between gold nanoparticles and ZnO nanorods with alternating oxygen and hydrogen treatments. This reversibility of the electron transfer under oxidative and reductive conditions is another important characteristic of the SMSI effect.[12,13,31,32]

EPR Studies. Electron paramagnetic resonance (EPR), a sensitive technique in detecting species with unpaired electron, was employed to study the electron transfer effect. Figure 2b revealed there were two signals for the ZnO nanorod support at g = 2.003 and g = 1.960. The weak signal at g = 2.003 can be ascribed to superoxide ions, and its intensity remained unchanged to the pretreatment conditions. The signal at g = 1.960 is assigned to singly ionized oxygen vacancy ($Vo^{\bullet}$).[33] When gold was supported on the surface of ZnO nanorods and pretreated under oxygen atmosphere, the paramagnetic defect ($Vo^{\bullet}$) disappeared. However, the signal at g = 1.960 appeared again (regain of unpaired electrons) when the sample was treated again under H_2 at 300 °C. There are three kinds of oxygen vacancies in ZnO: Vo^0, $Vo^{\bullet}$, and $Vo^{\bullet\bullet}$, among which the formation energy of $Vo^{\bullet\bullet}$ is the lowest and the $Vo^{\bullet}$ is metastable as reported in the literature.[33−35] Therefore, we propose that the $Vo^{\bullet}$ was converted back to the paramagnetically silent $Vo^{\bullet\bullet}$ which obtained an electron from gold when pretreated under oxidative conditions. After pretreated under reductive condition, the $Vo^{\bullet\bullet}$ returned an electron to gold and converted to paramagnetic $Vo^{\bullet}$. In consistence with the results of *in situ* DRIFTS, the EPR studies also established the reversibility of the electron transfer between gold and ZnO support under oxidative−reductive pretreatment atmosphere.

Catalytic Performance. CO oxidation is a simple and typical probe reaction for investigating the catalytic properties of gold. Therefore, we chose this reaction to study the effect of SMSI on the catalytic activity of Au/ZnO-nanorod. As shown in Figure 3a, the CO conversion increased when the pretreatment temperature was raised from 60 to 200 °C under oxygen atmosphere. We tested that the bare ZnO nanorod showed no catalytic activity from room temperature to 300 °C. According to the results of *in situ* DRIFTS (Figure 2a), the charges on the surfaces of gold nanoparticles became increasingly positive with increasing oxygen pretreatment temperature. However, the CO conversion decreased dramatically when the pretreatment temperature was increased to 300 °C (Figure 3a). The signal of super oxide in the EPR spectra (Figure 2b) did not change with the pretreatment temperature and atmosphere. Thus oxygen activation to superoxide is not the reason for decreased activity at 300 °C. Besides, the XRD patterns (Figure S5) and size distribution obtained by TEM images (Figure S3) of Au/ZnO-nanorod indicated constant sizes of gold nanoparticles. Therefore, the sintering of gold nanoparticles can also be excluded as the reason for the decreased catalytic performance. The decrease in catalytic activity might be due to encapsulation of active gold site (Figure 1c-d).

The reversibility (under oxidation and reduction) of the SMSI effect on the catalytic activity of Au/ZnO-nanorod in CO oxidation was also investigated. As shown in Figure 3b, the catalytic activities at room temperature for 200 °C-pretreated sample remains essentially unperturbed by changing the pretreatment atmosphere. When pretreated under reductive conditions at 300 °C, the room temperature CO conversions over Au/ZnO-nanorod decreased even more than those oxidatively treated sample. This may look unexpected because the thin layer of ZnO has already retreated and gold surfaces are exposed again after pretreated under H_2. It implies that the negative charge on the surface of gold has a detrimental effect to the catalytic activity. Electronic interaction with support does also play an important role in catalysis other than the geometric (migration of support) effect when SMSI phenomena appeared.

X-ray Absorption Fine Structure Studies. In order to further examine the interaction between gold nanoparticles and ZnO nanorods, extended X-ray absorption fine structure (EXAFS), and X-ray absorption near edge structure

dx.doi.org/10.1021/ja3033235 | J. Am. Chem. Soc. 2012, 134, 10251−10258

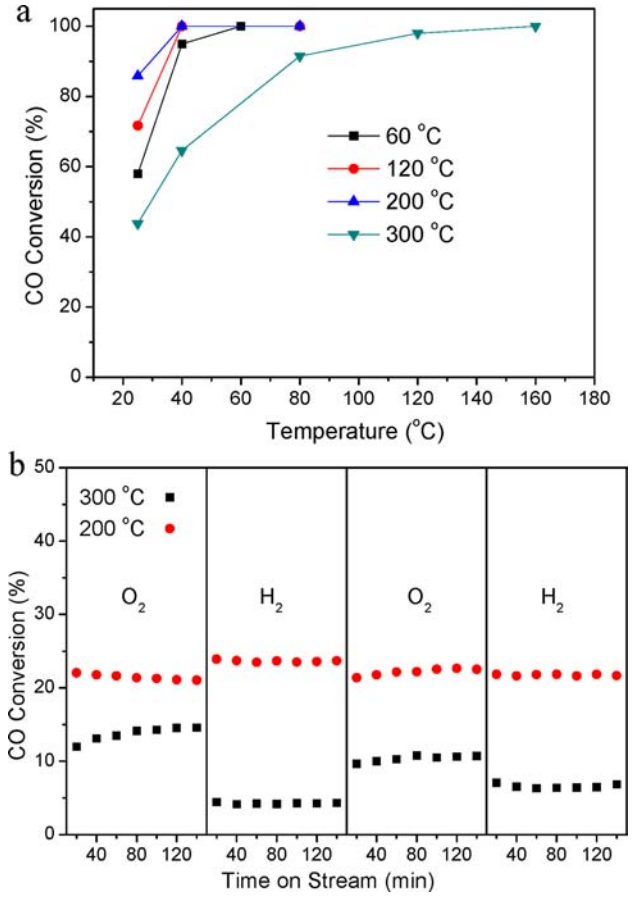

Figure 3. Catalytic performance in CO oxidation. The gas flow was composed of $CO/O_2/He$ (vol. ratio) = 1/6/93 with a flow rate of 30 mL•min^{-1}. (a) CO conversion with increasing temperature over Au/ZnO-nanorod pretreated under oxygen flow at 60 °C, 120 °C, 200 °C, and 300 °C. 60 mg of the catalyst was used. (b) CO conversions with time on stream at room temperature over the Au/ZnO-nanorod catalyst pretreated at 300 and 200 °C under O_2 and H_2 flow alternatively. Ten mg of the catalyst was used.

(XANES) spectra were measured on 20Au/ZnO-nanorod to probe the coordination environment and valence state of gold. We increased the loading of Au to 20 wt % for better *S*/*N* ratio in EXAFS experiments. After the 20Au/ZnO-nanorod sample was pretreated at 300 °C under oxygen or hydrogen atmosphere, and judging by the coordination number of gold (Table 1), the gold nanoparticles still remain small and the average particles size is 2−3 nm.[36] In the Fourier transform EXAFS data (r space, without phase correction, Figure 4a), for the oxygen pretreated sample, the first shell is attributed to the Au−O coordination. The extraordinarily short distance at ∼1.95 Å (Table 1) is ascribed to an Au(III)−O bond.[37] There are three peaks at longer distances (peaks 2, 3, and 4 in Figure 4a), which are fitted to be the Au−Zn (in AuZn alloy phase), Au−Au (in metallic state gold), and Au−Au/Au−O−Zn (in oxidative state gold), respectively, as listed in Table 1. The intensity of the Au−O peak (peak 1 in Figure 4a) decreased with increasing pretreatment temperature, and correspondingly, the coordination number of Au−O decreased from 3.6 to 1.5 (Table 1) and the average bond length of Au−Au also shortened from 3.35 Å (Au−O−Au bond) to 2.86 Å (Au−Au in Au(0)) as shown in Table 1 when the pretreatment temperature increased from 60 to 300 °C. This indicated at low treatment temperature gold mainly existed as oxide state, that is, there is an oxygen shell between two gold atoms, and it was gradually reduced to metallic state with increasing annealing temperature. This is consistent with the XANES spectra, as shown in Figure 4b, the intensity of the white line at Au L_{III}-edge decreased with increasing pretreatment temperature under oxygen atmosphere, indicating that the d band of the cationic gold is gradually occupied by electrons. Interestingly, by analyzing the EXAFS data in more details, we found there was Au−Zn interaction with a length of ∼3.10 Å when the pretreatment temperature was at 60, 120, and 200 °C under oxygen atmosphere. The distance (∼3.10 Å) is longer than that of Au−Zn bond in the alloy state (∼2.77 Å), so there should be an oxygen atom bridged between them; in other words, the Au−O−Zn interaction was formed at the interfaces of gold and ZnO nanorods.

Table 1. Analysis Results of the EXAFS Data at Au L_{III}-Edge[a]

sample	shell	N	R (Å)	$\sigma^2 \times 10^3$ (Å^2)	ΔE_0 (eV)	r-factor (%)	Δk (Å^{-1})	ΔR (Å)
Au foil	Au−Au	12	2.86	4.52	1.7	0.45	3.1−11.1	1.2−3.6
60	Au−O	3.6	1.95	0.42	6.2	1.34	3.1−11.1	1.2−3.6
	Au−Zn	0.8	3.10	2.88	6.2			
	Au−Au	2.3	3.35	2.88	6.2			
120	Au−O	3.6	1.96	2.57	7.3	0.52	3.1−11.1	1.2−3.6
	Au−Zn	2.4	3.16	2.57	7.3			
	Au−Au	2.8	3.05	2.57	7.3			
200	Au−O	3.3	1.94	2.65	4.4	0.60	3.1−11.1	1.2−3.6
	Au−Zn	2.0	3.10	5.64	4.4			
	Au−Au	2.8	2.93	5.64	4.4			
300	Au−O	1.5	1.95	3.00	2.75	1.12	3.1−11.1	1.2−3.4
	Au−Au	6.6	2.86	7.09	2.75			
300-H_2	Au−Zn	2.1	2.77	8.64	−0.48	1.53	2.9−10.8	2.0−3.4
	Au−Au	6.6	2.81	8.64	−0.48			

[a]The 20Au/ZnO-nanorod that was pretreated under O_2 atmosphere at 60 °C, 120 °C, 200 °C, and 300 °C and followed by pretreatment under H_2 atmosphere at 300 °C. N, the coordination number for the absorber-backscatterer pair. R, the average absorber−backscatterer distance. σ^2, the Debye−Waller factor. ΔE_0, the inner potential correction. Δk and ΔR are data range used for data fitting in k-space and R-space. The k^3-weighted EXAFS spectra at Au L_{III}-edge were shown in Figure S6.

dx.doi.org/10.1021/ja3033235 | J. Am. Chem. Soc. 2012, 134, 10251−10258

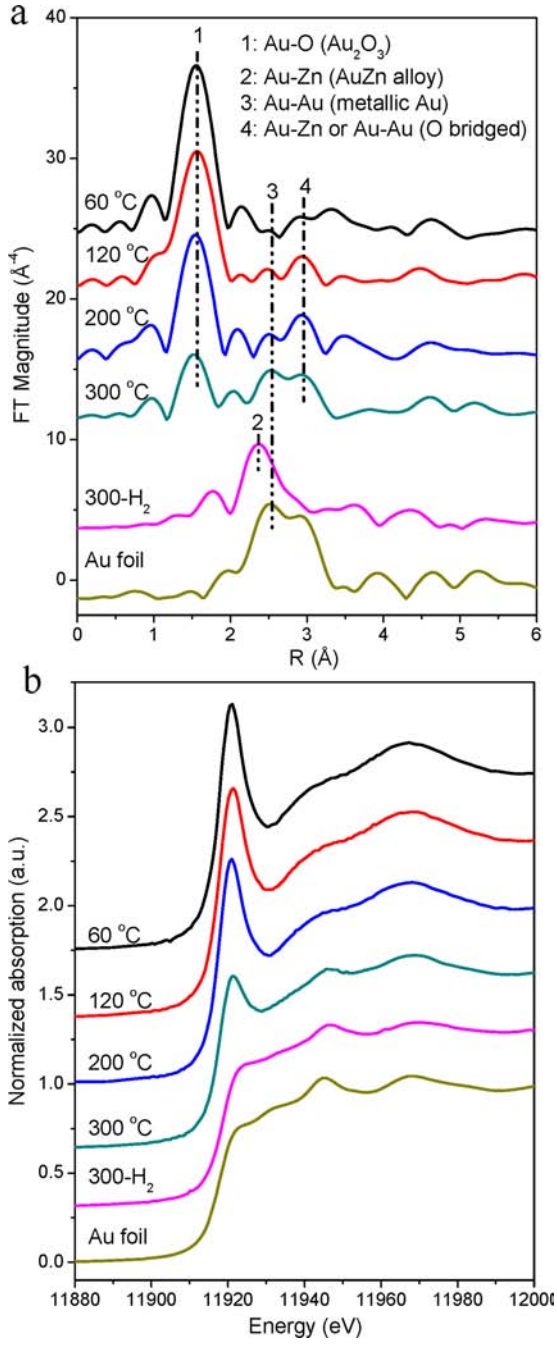

Figure 4. (a) Fourier transform of k^3-weighted EXAFS spectra (without phase correction) and (b) normalized XANES spectra at the Au L_{III}-edge of 20Au/ZnO-nanorod catalyst. The catalysts were pretreated under O_2 atmosphere at 60 °C, 120 °C, 200 °C, and 300 °C and followed by pretreatment under H_2 atmosphere at 300 °C.

We noticed that when the annealing temperature increased to 300 °C in the oxygen gas flow, there are still Au−O bonds with an average bond length of 1.95 Å and a smaller coordination number of 1.5. We ascribe it to the gold underneath the surface of gold nanoparticle and contacting intimately with the surface of ZnO. After reduction at 300 °C, there appears an Au−Zn peak (peak 2 in Figure 4a), which is ascribed to an AuZn alloy-like state. The corresponding intensity of the white line in the XANES spectra (Figure 4b) was close to that of Au foil which indicated that the d orbital of gold was almost fully occupied. Therefore, the retreat of ZnO on the surface of gold nanoparticles (Figure 1e-f and Figure S4) can be due to the formation of AuZn alloy at the interfaces. We also noticed that the Au−Au bond length (2.81 Å) is slightly shorter than that in metallic gold (2.86 Å). This might be caused by the contraction of the gold nanoparticles after formation of AuZn alloy.

X-ray Photoelectron Spectroscopy. We further employed X-ray photoelectron spectroscopy (XPS) to examine the valence state of Au. Figure 5 gives the XPS spectra of Au/ZnO under various pretreatment conditions. Although part of the peaks of Au $4f_{5/2}$ was overlapped by the signal of Zn 3p, we deconvoluted the branches of Au $4f_{7/2}$ of the gold peak. The general trend is clear; e.g. the amount of the metallic gold (Au(0)) increased when the pretreatment temperature was elevated. Correspondingly, the total ratio of the cationic gold (Au(I) and Au(III)) decreased (see Table S1 for results of quantitative fit). More than half of the Au on the surface existed as metallic state even when just dried at low temperature (60 °C), which reflects the instability of auric oxides that can be reduced under oxygen atmosphere even at room temperature.[38] The atomic ratio of Au/Zn remained roughly constant from pretreatment temperature of 60 to 200 °C but decreased sharply (from 0.52 to 0.30) when the pretreatment temperature increases from 200 to 300 °C (Table S1). This also provides strong evidence that the gold nanoparticles were covered by ZnO thin layer. After further pretreatment at 300 °C under hydrogen atmosphere, the atomic ratio of Au and Zn was 0.32. This may be due to the formation of AuZn alloy at the interfaces and the sinking of some gold nanoparticles into the ZnO (Figure 1f and Figure S4).

We have observed the existence of cationic gold in XPS, XANES, and EXAFS (the short Au−O bond). However, no DRIFTS signal of CO adsorption on cationic gold was detected. These observations indicated that the cationic charged gold mainly lay underneath and near the contact between gold and ZnO surface and has no direct access to CO, while the gold in metallic state was concentrated on the top surface of gold nanoparticles and was slightly positively charged when pretreated at increasing temperature under oxygen atmosphere due to transfer of some electrons to the support, as pictured in Figure 6.

In Figure 6, we do see the possibility that the electronic effect in catalysis is due not just to the Au nanoparticles itself, but the interfacial atoms of Au(III) interacting strongly with the ZnO "ligand" to fine-tune the electronic structure on surface gold which in turn affect chemisorptions of the surface gold.

DISCUSSION

In above, we have demonstrated that the SMSI states do exist in ZnO-nanorod supported gold nanocatalysts. It exhibits many of the characteristics of the classical SMSI in the supported group VIII metals:[12,13,26,39] (a) response of higher temperature pretreatment; (b) encapsulation of metals by the substrates; (c) reduction of CO adsorption and catalytic activity; (d) occurrence of electron transfer between metals and substrates; and (e) reversibility under oxidative or reductive pretreatment conditions. However, the pretreatment atmosphere is quite different: in the Au/ZnO-nanorod system, oxygen was needed while in the classical SMSI such as Pt(Pd)/TiO_2 system, hydrogen reduction is necessary. The contrasts were listed in Table S2. In the classical SMSI state, when pretreated under H_2 atmosphere, the Fermi level of the partially reduced metal oxide support becomes higher than that of the metal nanoparticles.[13]

dx.doi.org/10.1021/ja3033235 | J. Am. Chem. Soc. 2012, 134, 10251−10258

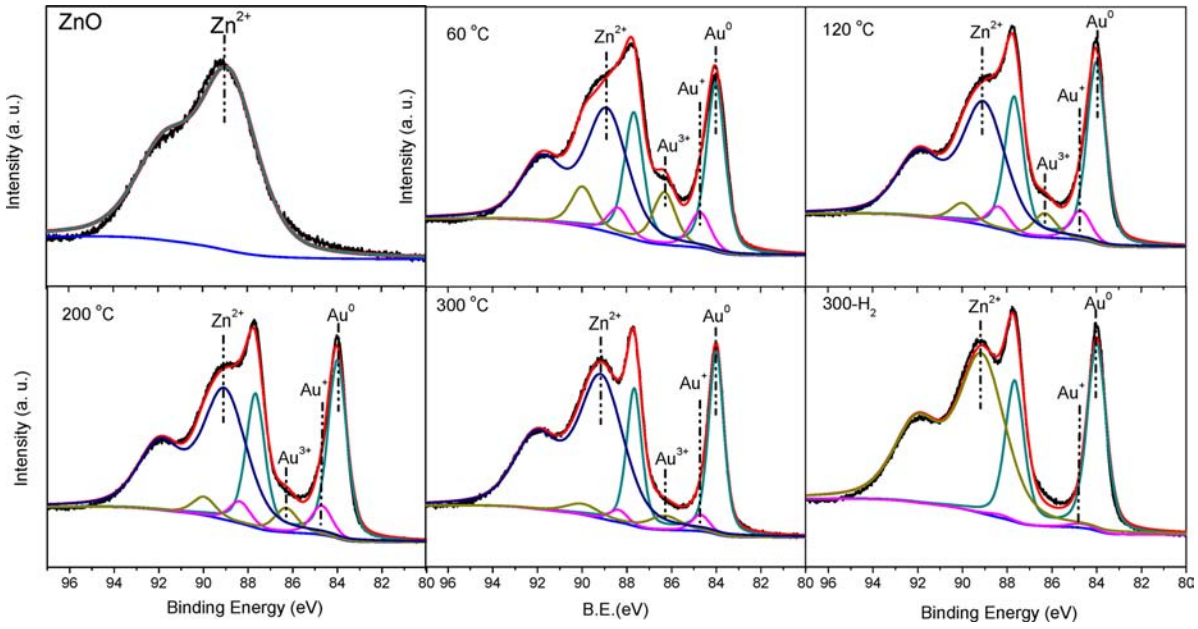

Figure 5. XPS spectra of Zn 3p and Au 4f of Au/ZnO-nanorod catalyst. The catalysts were pretreated under O_2 atmosphere at 60 °C, 120 °C, 200 °C, and 300 °C and followed by pretreatment under H_2 atmosphere at 300 °C.

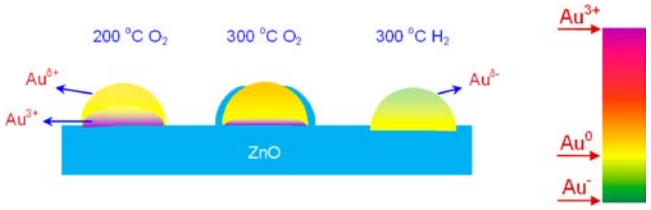

Figure 6. Schematic illustration for the SMSI states in the Au/ZnO-nanorod system under various pretreatments. The color bar depicts the sign and degree of charging of the gold nanoparticles.

Therefore, the electron would transfer from the support to the metal nanoparticles in order to attain a Fermi-level equilibration at the interfaces. In our case, when pretreated with oxygen, the Fermi level of ZnO was lower than that of gold nanoparticles, which would facilitate the electron transfer from the gold nanoparticles to the support.[40−42] Considering the above difference, we denote the SMSI which occurred under oxidative condition at 300 °C as O-SMSI in order to distinguish it from the classical SMSI.

It is now apparent the strong interaction between gold and ZnO has imparted different chemical properties on both metal and support. On the gold side, because of the ZnO underneath, cationic gold (in particular Au(III)) becomes stabilized under oxidative treatment at mild temperature. On the other hand, Au(III) was reduced to Au(0) on the top free side of gold. On the ZnO side, the normally stable Zn(II) could be reduced by hydrogen at 300 °C to form AuZn alloy because of the intimate contact with gold. If one refers to interaction between metal and support as SMSI by the two necessary criterions: (a) electron transfer between them and (b) increased contact between metal and support, there are actually two kinds of SMSI in Au/ZnO reported here termed as R-SMSI and O-SMSI. The R-SMSI is caused by hydrogen reduction condition at the temperature of 300 °C; the electron transfer is from support to metal and gold nanoparticles sunk under the surface of ZnO or formed AuZn alloy to increase contact. In O-SMSI, which occurred under oxidative condition at 300 °C, the electron transfer is from metal to support and ZnO moved on top of Au to encapsulate it. The two cases are reversible, by switching between oxygen and hydrogen treatment. While the direction of electron transfer in R-SMSI is in agreement with the classical SMSI in group VIII elements, the decoration of Au with support occurred in O-SMSI, as shown in Table S2. It is also interesting to observe that R-SMSI in our Au/ZnO system is characterized by the formation of AuZn alloy, the epitaxial interaction between gold and ZnO, and some sinking of gold nanoparticles, which is partly similar with that of the classical SMSI, although encapsulation of gold by ZnO does not occur.

In this work, we observed an enhanced activity of CO oxidation after oxidative pretreatment at low temperature (without encapsulation). This may be due to the partially positively charged Au(0) surface for better CO activation. Trivalent Au(III) species exist between ZnO and Au nanoparticle to help the SMSI between them. The interaction between gold atoms and ZnO nanorods at the interfaces plays an important role in influencing the cataltytic performances. Previous works by the Gates group did show the importance of Au(III) on interface in influencing catalysis.[43,44] Recently, Yates and co-workers further showed the crucial Au/TiO_2 interface for activating $CO\text{-}O_2$.[45] On the other hand, the R-SMSI state, giving a negatively charged gold surface, may be active in other catalytic reactions such as hydrogenation. This needs to be explored further in the future.

The phenomenon of SMSI was originally observed in the TiO_2 supported Pt system, where the support exhibited variable valences. Therefore, the accumulation of electron on support located at the interfaces was thought to be the driving force for the migration of the TiO_2 to the surface of Pt nanoparticles under reductive conditions.[12,13,39] However, in systems of gold supported on metallic oxides with variable valences (e.g., TiO_2, CeO_2, etc.), no encapsulation of the gold nanoparticles by the support have been reported.[31,32,46] In contrast, we find the O-SMSI or R-SMSI in the Au/ZnO system does invoke the change of charge distribution and mass transport. In O-SMSI, the formation of the Au−O−Zn linkage under the oxidative

dx.doi.org/10.1021/ja3033235 | J. Am. Chem. Soc. 2012, 134, 10251−10258

pretreatment may have played a crucial role in driving the ZnO to decorate the surface of gold nanoparticles; while in the R-SMSI, the formation of Au−Zn alloy might be very important. Also the rich defects on the nonpolar surface of ZnO nanorod[47] or the properties of the n-type semiconductor might also play a role in influencing the SMSI between gold and the ZnO substrate. Further study is needed to clarify the real driving force for the O-SMSI or R-SMSI.

Although the SMSI effect was discovered and applied on CO oxidation for the Au/ZnO system in this work, there will be several implications in the general field of gold nanocatalysts. First, the strong interaction between Au and support will allow very stable catalyst which is important in any industrial applications. Second, a precise control of small-sized gold nanoparticles will be more feasible in the future. This is particularly significant for gold-catalyzed organic reactions which often need sub2 nm gold clusters.[48,49] Third, the charge state of supported gold may be controlled with careful oxidative/reductive pretreatment which will be important in controlling catalytic activity and selectivity of Au-catalyzed reactions.

■ CONCLUSIONS

In summary, we have presented two kinds of SMSI (O-SMSI and R-SMSI) between gold nanoparticles and ZnO nanorods. The O-SMSI state appeared in our Au/ZnO system was in opposite sense (direction of electron transfer and encapsulation condition) in comparison with the classical SMSI observed in the supported group VIII metals. The R-SMSI state in Au/ZnO occurred under the same reductive pretreatment conditions as the classical SMSI, but it gave a lower activity in CO oxidation. In CO oxidation, we found that O-SMSI state associated with positively charged gold nanoparticles has strong effect on its catalytic activity before and after encapsulation. The catalytic mechanism of the supported gold nanoparticles is complicated by many factors including the effects of particle sizes and the nature of the support.[5,50] We believe our discovery of the O-SMSI and R-SMSI effects in Au/ZnO nanorods provides a new way to control the interaction between gold and the support as well as catalytic activity.

■ EXPERIMENTAL SECTION

Synthesis of ZnO Nanorods. Typical synthesis method was according to previous literature with slight modification.[21] Briefly, 210 mL of the aqueous solution containing $Zn(NO_3)_2$ (0.105 mol) and NaOH (2.1 mol) was prepared freshly. Then it was diluted by 1050 mL of 99.9% ethanol as quickly as possible in order to slow down the growth rate of ZnO nanocrystals. Subsequently, 4.2 g of CTABr (0.011 mol) and 105 mL of EDA (ca. 1.56 mol) were dissolved into the diluted precursor solution and stirred vigorously for 5 days at room temperature. The as-prepared ZnO nanorods were washed with 95% ethanol and deionized water for several times by centrifugation. The white color precipitated products were dried in the oven at 60 °C for 12 h and followed by calcination at 560 °C in air for 6 h to remove the organic compounds.

Synthesis of Au/ZnO-Nanorod. The deposition of gold on the ZnO nanorods was synthesized by the deposition-precipitation method. The pH value of 10 mL of $HAuCl_4$ aqueous solution (Au: 5.0 wt %) was tuned to ~7.0 by Na_2CO_3 (0.1 M). Then it was added dropwise into the aqueous suspension of 1 g of ZnO nanorods in 10 mL of deionized water. The pH value of the mixture was kept at 9.0−9.5. After being stirred for 48 h at room temperature, the mixture was centrifugated and washed with deionized water until there is no Cl^- detected by the $AgNO_3$ solution, and then the as-prepared catalyst was divided into two parts and dried at 60 and 120 °C for 12 h in oven, respectively. The actual loading of gold analyzed by ICP/MS was 4.9 wt %, which was close to the nominal value (5.0 wt %). This sample is denoted as Au/ZnO-nanorod. In order to do the XANES and EXAFS experiment, we increased the loading of gold to 20 wt %, the actual loading of which is 20.8 wt %. This sample is denoted as 20Au/ZnO-nanorod.

Catalytic Performances in CO Oxidation Reaction. The CO oxidation reaction was carried out in a fix-bed flow reactor system. A gaseous mixture of CO (1 vol%) and O_2 (6 vol%) balanced with He was allowed to pass through 60 mg of the catalyst at a total flow rate of 30 mL•min^{-1} (corresponding to a space velocity of 30,000 mL•g_{cat}^{-1}•h^{-1}). Prior to the reaction, the catalyst was pretreated with 10 vol% O_2 in He (flow rate: 30 mL•min^{-1}) at different temperatures for 1 h and then cooled to the room temperature under He. The reactant gases (CO, O_2) were purified by 4 Å molecular sieves and then mixed before entering the reactor. The inlet and outlet gas compositions were online analyzed by a gas chromatograph (HP 6820) equipped with a Carboxen 1000 column and a thermal conductivity detector (TCD).

Characterization. Chemical compositions of the Au/ZnO-nanorod were determined by inductively coupled plasma mass spectrometry (ICP/MS) on an ELAN6000 instrument (Perkin-Elmer Corporation). The morphology of the Au/ZnO-nanorod was characterized by field emission scanning electron microscope (FESEM, JEOL JSM-7600). HRTEM images were obtained on a transmission electron microscope operating at 200 kV (FEI Tecnai 20 G^2 S-Twin). For the TEM sample preparation, ZnO nanorods with or without gold deposition were dispersed in 95% ethanol, and then several drops of the suspension were put on microgrid carbon polymer supported on copper grid. After drying, it was ready for the TEM observations.

The DRIFT spectra were collected by using a commercial instrument (Nicolet 6700) equipped with a MCT detector. The spectrum was obtained by collecting 64 scans at a resolution of 4 cm^{-1}. Twenty mg of a catalyst sample was loaded into the cell with a ZnSe window which can work at high temperature. Prior to CO adsorption, the sample was *in situ* pretreated in 10 vol% O_2/He for 1 h at different temperatures and then cooled to room temperature. The gas flow was switched to pure He for collecting the background spectrum. Subsequently, the sample was exposed to a flowing mixture of 5 vol % CO in Ar with a rate of 30 mL·min^{-1} for 30 min. After purged with pure He for 2 min, the CO in the gaseous mixture was flushed, and the spectrum was collected again.

The EPR spectra were recorded at 77 K with a Bruker EMX 10/12 spectrometer working in the X-band (9.53 GHz). A weighted catalyst sample of 5 mg was placed inside a 4-mm O.D. quartz tube with greaseless stopcocks. Before collecting data, the sample was first evacuated at room temperature until the residual pressure lower than 10^{-3} Torr and then put in Dewar flasks to decrease the temperature to 77 K.

The surface Au/Zn atomic ratios, along with the binding energies of Au 4f and Zn 3p, were determined by synchrotron-based XPS measurements carried out at beamline 20A1 of the National Synchrotron Radiation Research Center (NSRRC) in Taiwan. The XPS spectra were measured in an UHV chamber with a base pressure ~5 × 10^{-10} Torr equipped with a CLAM-4 9-channeltron hemispherical electron energy analyzer (VG Microtech). Fixed photon energy of 400 eV was utilized to measure the Au 4f core level spectra. The total energy resolution, including the beamline and electron energy analyzer, was estimated to be ~0.3 eV. The binding energy scale was referenced to the pronounced Au $4f_{7/2}$ peak of a reference Au foil at 84 eV. The recorded spectra were fit by a least-squares procedure to a product of Gaussian−Lorentzian functions after subtraction of background. The concentration of each element was calculated from the area of the corresponding peak, calibrated with the atomic sensitivity factor.

XANES spectra at Au L_{III}-edge were recorded at beamline 17C1 of the NSRRC in Taiwan. The electron storage ring is operated at 1.5 GeV and a beam current of 360 mA with a top-up injection mode. The beamline employs a double Si(111)-crystal monochromator for energy

dx.doi.org/10.1021/ja3033235 | J. Am. Chem. Soc. 2012, 134, 10251−10258

selection with a resolution $\Delta E/E$ better than 2 * 10^{-4}. The powdery catalysts were treated at different temperature under air atmosphere and then stuck on Scotch tap. All spectra were recorded at room temperature in a fluorescence mode. Au foil as standard compound was measured simultaneously by using the third ionization chamber so that energy calibration could be performed. The X-ray absorption data were processed by Athena software package.[51]

■ ASSOCIATED CONTENT

Supporting Information

Properties of ZnO nanorods, additional characterizations of gold nanoparticles, XPS analysis results, and contrasts between classical SMSI and that of Au/ZnO. This material is available free of charge via the Internet at http://pubs.acs.org.

■ AUTHOR INFORMATION

Corresponding Author

cymou@ntu.edu.tw

Notes

The authors declare no competing financial interest.

■ ACKNOWLEDGMENTS

This research was supported by grants from National Science Council of Taiwan and National Taiwan University for a postdoctorial fellowship (X. Liu). We thank National Synchrotron Radiation Research Center (NSRRC) of Taiwan for generous beamtime allocation.

■ REFERENCES

(1) Haruta, M.; Kobayashi, T.; Sano, H.; Yamada, N. *Chem. Lett.* **1987**, 405.
(2) Freund, H. J.; Meijer, G.; Scheffler, M.; Schlogl, R.; Wolf, M. *Angew. Chem., Int. Ed.* **2011**, *50*, 10064.
(3) Haruta, M. *Catal. Today* **1997**, *36*, 153.
(4) Park, E. D.; Lee, J. S. *J. Catal.* **1999**, *186*, 1.
(5) Liu, Y.; Jia, C. J.; Yamasaki, J.; Terasaki, O.; Schuth, F. *Angew. Chem., Int. Ed.* **2010**, *49*, 5771.
(6) Wang, L.-C.; He, L.; Liu, Y.-M.; Cao, Y.; He, H.-Y.; Fan, K.-N.; Zhuang, J.-H. *J. Catal.* **2009**, *264*, 145.
(7) Chen, M. S.; Goodman, D. W. *Science* **2004**, *306*, 252.
(8) Schuth, F.; Galeano, C.; Guttel, R.; Paul, M.; Arnal, P.; Lu, A. H. *Chem.—Eur. J.* **2011**, *17*, 8434.
(9) Lin, C. H.; Liu, X. Y.; Wu, S. H.; Liu, K. H.; Mou, C. Y. *J. Phys. Chem. Lett.* **2011**, *2*, 2984.
(10) Zheng, N. F.; Huang, X. Q.; Guo, C. Y.; Zuo, L. Q.; Stucky, G. D. *Small* **2009**, *5*, 361.
(11) Yin, H. F.; Ma, Z.; Zhu, H. G.; Chi, M. F.; Dai, S. *Appl. Catal., A* **2010**, *386*, 147.
(12) Tauster, S. J.; Fung, S. C.; Garten, R. L. *J. Am. Chem. Soc.* **1978**, *100*, 170.
(13) Fu, Q.; Wagner, T. *Surf. Sci. Rep.* **2007**, *62*, 431.
(14) Qiao, B. T.; Wang, A. Q.; Yang, X. F.; Allard, L. F.; Jiang, Z.; Cui, Y. T.; Liu, J. Y.; Li, J.; Zhang, T. *Nat. Chem.* **2011**, *3*, 634.
(15) Van, T. T. H.; Pan, C. J.; Rick, J.; Su, W. N.; Hwang, B. J. *J. Am. Chem. Soc.* **2011**, *133*, 11716.
(16) Hervier, A.; Baker, L. R.; Komvopoulos, K.; Somorjai, G. A. *J. Phys. Chem. C* **2011**, *115*, 22960.
(17) Kamiuchi, N.; Matsui, T.; Kikuchi, R.; Eguchi, K. *J. Phys. Chem. C* **2007**, *111*, 16470.
(18) Caballero, A.; Holgado, J. P.; Gonzalez-delaCruz, V. M.; Habas, S. E.; Herranz, T.; Salmeron, M. *Chem. Commun.* **2010**, *46*, 1097.
(19) Meyer, R.; Lemire, C.; Shaikhutdinov, S. K.; Freund, H.-J. *Gold Bull.* **2004**, *37*, 72.
(20) Fu, Q.; Wagner, T.; Olliges, S.; Carstanjen, H. D. *J. Phys. Chem. B* **2005**, *109*, 944.
(21) Liu, B.; Zeng, H. C. *Langmuir* **2004**, *20*, 4196.
(22) Li, G. R.; Hu, T.; Pan, G. L.; Yan, T. Y.; Gao, X. P.; Zhu, H. Y. *J. Phys. Chem. C* **2008**, *112*, 11859.
(23) Haruta, M. *Chem. Rec.* **2003**, *3*, 75.
(24) Herzing, A. A.; Kiely, C. J.; Carley, A. F.; Landon, P.; Hutchings, G. J. *Science* **2008**, *321*, 1331.
(25) Akita, T.; Lu, P.; Ichikawa, S.; Tanaka, K.; Haruta, M. *Surf. Interface Anal.* **2001**, *31*, 73.
(26) Liu, J. Y. *ChemCatChem* **2011**, *3*, 934.
(27) Carabineiro, S. A. C.; Machado, B. F.; Bacsa, R. R.; Serp, P.; Drazic, G.; Faria, J. L.; Figueiredo, J. L. *J. Catal.* **2010**, *273*, 191.
(28) Castillejos, E.; Bacsa, R.; Guerrero-Ruiz, A.; Rodriguez-Ramos, I.; Datas, L.; Serp, P. *Nanoscale* **2011**, *3*, 929.
(29) Mihaylov, M.; Knozinger, H.; Hadjiivanov, K.; Gates, B. C. *Chem. Ing. Tech.* **2007**, *79*, 795.
(30) Boronat, M.; Concepcion, P.; Corma, A. *J. Phys. Chem. C* **2009**, *113*, 16772.
(31) Huang, X. S.; Sun, H.; Wang, L. C.; Liu, Y. M.; Fan, K. N.; Cao, Y. *Appl. Catal., B* **2009**, *90*, 224.
(32) Cies, J. M.; del Rio, E.; Lopez-Haro, M.; Delgado, J. J.; Blanco, G.; Collins, S.; Calvino, J. J.; Bernal, S. *Angew. Chem., Int. Ed.* **2010**, *49*, 9744.
(33) Vanheusden, K.; Warren, W. L.; Seager, C. H.; Tallant, D. R.; Voigt, J. A.; Gnade, B. E. *J. Appl. Phys.* **1996**, *79*, 7983.
(34) Oba, F.; Choi, M.; Togo, A.; Tanaka, I. *Sci. Technol. Adv. Mater.* **2011**, *12*, 034302.
(35) Oba, F.; Togo, A.; Tanaka, I.; Paier, J.; Kresse, G. *Phys. Rev. B* **2008**, *77*, 245202.
(36) Frenkel, A. I.; Hills, C. W.; Nuzzo, R. G. *J. Phys. Chem. B* **2001**, *105*, 12689.
(37) Bus, E.; Prins, R.; van Bokhoven, J. A. *Phys. Chem. Chem. Phys.* **2007**, *9*, 3312.
(38) Ono, L. K.; Cuenya, B. R. *J. Phys. Chem. C* **2008**, *112*, 4676.
(39) Tauster, S. J. *Acc. Chem. Res.* **1987**, *20*, 389.
(40) Fu, Q.; Saltsburg, H.; Flytzani-Stephanopoulos, M. *Science* **2003**, *301*, 935.
(41) Subramanian, V.; Wolf, E. E.; Kamat, P. V. *J. Phys. Chem. B* **2003**, *107*, 7479.
(42) Wang, X. D.; Summers, C. J.; Wang, Z. L. *Appl. Phys. Lett.* **2005**, *86*, 013111.
(43) Fierro-Gonzalez, J. C.; Guzman, J.; Gates, B. C. *Top. Catal.* **2007**, *44*, 103.
(44) Fierro-Gonzalez, J. C.; Gates, B. C. *Chem. Soc. Rev.* **2008**, *37*, 2127.
(45) Yates, J. T.; Green, I. X.; Tang, W. J.; Neurock, M. *Science* **2011**, *333*, 736.
(46) Goodman, D. W. *Catal. Lett.* **2005**, *99*, 1.
(47) Lopez, N.; Norskov, J. K. *Surf. Sci.* **2002**, *515*, 175.
(48) Haruta, M.; Huang, J. H.; Akita, T.; Faye, J.; Fujitani, T.; Takei, T. *Angew. Chem., Int. Ed.* **2009**, *48*, 7862.
(49) Haruta, M.; Ishida, T.; Nagaoka, M.; Akita, T. *Chem.—Eur. J.* **2008**, *14*, 8456.
(50) Bond, G.; Thompson, D. *Gold Bull.* **2009**, *42*, 247.
(51) Ravel, B.; Newville, M. *J. Synchrotron Radiat.* **2005**, *12*, 537.